The stiffness of circular joints and its effect on the deformation of the tunnel segmental lining along the longitudinal direction

Tunnelling for a Better Life – Yan, Celestino, Thewes & Eberhardt (Eds)

The stiffness of circular joints and its effect on the deformation of the tunnel segmental lining along the longitudinal direction

Xin Han*
School of Highway, Chang'an University, Xi'an, China
Department of Environment, Land and Infrastructure Engineering (DIATI), Politecnico di Torino, Turin, Italy

Fei Ye
School of Highway, Chang'an University, Xi'an, China

Pierpaolo Oreste
Department of Environment, Land and Infrastructure Engineering (DIATI), Politecnico di Torino, Turin, Italy

ABSTRACT: When analysing the damage phenomenon (crack, seepage, et al.) of a segmental lining during tunnel construction, its movement and deformation along the longitudinal direction is a critical aspect to be studied. Since the segmental lining is assembled by segments and using connecting bolts, there are many joints in the lining, which are the weak part of the lining and have an obvious deformation under the application of construction loads. This paper focuses on the circular joint which has a great influence on the segmental lining deformation along the longitudinal direction. Firstly, the evaluation methods of the bending stiffness and shear stiffness of a circular joint are developed; and then, based on the interaction between the connecting bolt and its hole, the methods for the evaluation of the shear stiffness of a single bolt and the one of the whole circular joint are proposed; finally, the segmental lining deformation along the longitudinal direction is analysed and the main factors are discussed.

Keywords: Tunnel segmental lining, Circular joint, Shear Stiffness, Bending Stiffness, lining behaviour in the longitudinal direction, Connecting Bolts, Bolt/Bolt hole interaction, Finite Element Method (FEM), Numerical Methods

1 INTRODUCTION

Segmental lining is widely used to support the surrounding ground when the tunnel boring machines (TBM) is adopted for the tunnel construction. Since the segmental lining consists of segments and connecting bolts, there are many joints that influence its behaviour. During the construction of the tunnel, the crack and seepage can be observed inside the lining (Gong et al., 2020; Lu, 2020), and the uplift movement of the segmental lining is a common phenomenon (Zhou and Ji, 2014).

In order to understand the reasons of the crack and seepage inside the lining, the segmental lining deformations along the longitudinal direction are widely studied using numerical models and analytical solutions (Chen et al., 2018; Cheng et al., 2021). Regarding this type of analysis, the influence of the circular joints is fundamental. Shiba et al. (1988) proposed the equation for the joint bending stiffness. Li et al. (2019) carried out a laboratory test to evaluate the joint stiffness under the application of a normal forces and moment. Cheng et al. (2021) suggested the general solution for the segmental lining deformation. Based on laboratory test, researchers (Guo et al., 2023a; Guo et al., 2023b; Liu et al., 2018) tested the bending and shear deformation of joints in the detailed; they further explained the nonlinear behaviour of the joint due to the nonlinear properties of the constituent materials.

In this paper the methods used to determine the variable joint bending and shear stiffnesses of the circular joints are introduced. Furthermore, a FEM model is developed to calculate the segmental lining deformation along the longitudinal direction and an iterative procedure is proposed in order to correctly consider the variable joint stiffness values. Using the proposed

*Corresponding author: hanxin@chd.edu.cn

DOI: 10.1201/9781003495505-142

method, deformations of rings and joints can be evaluated separately, and the nonlinear deformation of the tunnel segmental lining can be researched.

2 STIFFNESS OF THE CIRCULAR JOINT

When the tunnel segmental lining has a deformation along the longitudinal direction, the stiffness of the circular joints shows a nonlinear behaviour with the increase of the joint deformation. The methods adopted to calculate the bending and the shear stiffnesses of the circular joints are discussed in this section.

2.1 *Bending stiffness*

The bending stiffness of a circular joint is affected by the state of the joint, which can be described by the location of the neutral axis: it can be represented by the angle φ introduced by Shiba et al. (1988) and is determined by the existing normal force and the applied moment. There are two kinds of circular joint states: open and closed. When the joint is closed, the segments are connected each other, and the bending stiffness of the joint is the same of the lining segment. The limit moment M_{lim} of the circular joint before opening can be determined by the normal force N with the following equation:

$$M_{lim} = \frac{N \cdot I}{A \cdot R_e} \tag{1}$$

where I is the inertia moment of the ring cross-section, A and R_e are the cross-sectional area and the external radius of the ring, respectively.

When the joint is open, the bending stiffness of the joint show a nonlinear behaviour. The influence of the moment and of the normal force can be represented by a parameter λ,

$$\lambda = \frac{N \cdot (D_e - t)}{4 \cdot M} \tag{2}$$

where D_e is the external diameter of the tunnel, t is the thickness of the lining.

The equivalent bending stiffness $(EI)_{eq}$ of the joint can be obtained by the following equation (Han et al., 2023a):

$$(EI)_{eq} = \left[K_{com} \cdot \left(\frac{\pi}{2} - \varphi - \sin\varphi \cdot \cos\varphi\right) + K_{ten} \cdot \left(\frac{\pi}{2} + \varphi + \sin\varphi \cdot \cos\varphi\right)\right] \cdot \frac{(D_e - t)^3 \cdot t}{16} \cdot L_{b,p} \tag{3}$$

where $L_{b,p}$ is the projection length of the bolt, and K_{ten} are the tensile stiffness and compression stiffness of the joint:

$$\begin{cases} K_{com} = \frac{2 \cdot E_{con}}{L_{b,p}} \\ K_{ten} = \frac{2 \cdot E_b}{l_b} \cdot \frac{n \cdot A_b}{A} \end{cases} \tag{4}$$

where E_{con} is the elastic modulus of concrete, E_b is the elastic modulus of the bolt steel, l_b is the length of the bolt, n is the number of connecting bolts in the circular joint and A_b is the cross-sectional area of the connecting bolt.

In Equation 3, when the normal force is equal to 0, the angle φ can be obtained by the following simplified equation:

$$\varphi + cot\varphi = \pi \cdot \left(\frac{1}{2} + \frac{K_{ten}}{K_{com} - K_{ten}}\right) \tag{5}$$

When the normal force is larger than 0, the angle φ can be derived on the basis of Equation 2:

$$\lambda = \frac{2 \cdot m \cdot (\cos\varphi + \varphi \cdot \sin\varphi) - \pi \cdot \sin\varphi}{-2 \cdot m \cdot (\varphi + \cos\varphi \cdot \sin\varphi) + \pi} \tag{6}$$

where m can be determined by K_{com} and K_{ten}:

$$m = \frac{K_{com} - K_{ten}}{K_{com} + K_{ten}} \tag{7}$$

Furthermore, the equivalent bending stiffness of the joint also can be rewritten with the ratio between the equivalent bending stiffness of the joint and the one of the segmental lining ring:

$$(EI)_{eq} = \mathrm{JBSE}_{Boltz} \cdot E_{con} \cdot I \tag{8}$$

where JBSE_{Boltz} is the joint bending stiffness efficiency based on the Boltzmann function; it is equal to the ratio of the bending stiffnesses between the joint and the ring, and it can be considered as a modifying parameter of the bending stiffness of the lining ring.

JBSE_{Boltz} is a function of the λ parameter:

$$\mathrm{JBSE}_{Boltz} = \frac{(A_1 - A_2) \cdot \alpha}{1 + e^{(\lambda - \lambda_0)/q}} + A_2 + \Delta \tag{9}$$

where A_1, A_2, λ_0 and k are the basic parameters, α and Δ are the modified parameters. The detailed derivation of these parameters can be found in the reference (Han et al., 2023c):

A_1 is the lower value of the modified parameter JBSE_{Boltz}, which can be obtained by Equation 3 and Equation 4 when the normal force is equal to 0;

A_2 is the upper value of JBSE_{Boltz} which is equal to 1;

λ_0 is the specific value of λ when JBSE_{Boltz} is equal to $(A_1 + A_2)/2$, where the equivalent bending stiffness of the joint $(EI)_{eq}$ can be obtained by Equation 5, the angle φ can be derived by Equation 3, and λ_0 can be calculated by Equation 6;

q is a constant value, and can be obtained by the following equation:

$$q = \frac{A_2 - A_1}{4 \cdot \mathrm{JBSE}'} \tag{10}$$

where JBSE'is the slope of the centre point (λ_0, (A_1 +A_2)/2), which can be obtained by two adjacent points with a tiny increase $\Delta\lambda$, where the ordinate value of $JBSE_{Boltz}$ can be obtained on the abscissa value and $\lambda_0 + \Delta\lambda$ based on Equation 3, Equation 5 and Equation 8;

α and Δ are the modified parameters and can be obtained by the following equations:

$$\alpha = \frac{\left(1 + e^{(1-\lambda_0)/k}\right) \cdot \left(1 + e^{(-\lambda_0)/k}\right)}{e^{(1-\lambda_0)/k} - e^{(-\lambda_0)/k}} \tag{11}$$

$$\Delta = -\frac{(A_1 - A_2) \cdot \alpha}{1 + e^{(1-\lambda_0)/k}} \tag{12}$$

Based on Equation 3 and Equation 8, the equivalent bending stiffness of the joint can be calculated separately. The results are shown in Figure 1 referring to a well-known case of a shield tunnel (Zhou and Ji, 2014), and the results by the two methods show a very good consistence.

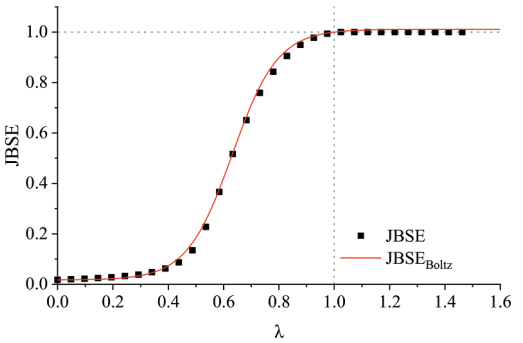

Figure 1. The trend of the joint bending stiffness based on the Equation 3 and Equation 8 calculation for a well-known case of a shield tunnel (Han et al., 2023c; Zhou and Ji, 2014).

2.2 *Shear stiffness*

The shear stiffness of a joint is influenced by the relative displacement of segments. Since the connecting bolts are installed along the circular joint, the inclination angle of the bolts varies with the location of the bolts on the circular joint. The shear stiffnesses of a single bolt and of the whole circular joint are here discussed separately.

2.2.1 *Shear stiffness of a single connecting bolt*

Based on the Timoshenko theory, the equivalent shear stiffness of a joint $(k \cdot G \cdot A)_{eq}$ is equal to the ratio between the shear force V_{total} applied on the joint and the corresponding relative displacement v_{seg} together with the projection length of the connecting bolt L_{bp}.

$$(k.G.A)_{eq} = \frac{V_{total}}{v_{seg}} .L_{bp} \tag{13}$$

When the segments have a relative displacement along the joint Δv_{seg}, the ratio between the increasement of the applied shear force ΔV_{total} and the corresponding relative displacement can be defined as shear stiffness K_{eq}:

$$K_{eq} = \frac{\Delta V_{total}}{\Delta v_{seg}} \tag{14}$$

where the applied shear force on the joint ΔV_{total} is equal to the shear force of the bolt on the cross section along the joint.

Furthermore, considering the inclination angle of the connecting bolt, the equivalent shear stiffness of the joint is the combination of the joint-bolt tensile stiffness and the joint-bolt shear stiffness when only the bolt is considered during the shear deformation (Han et al., 2023d):

$$K_{eq} = K_{eq,Q} \cdot \cos^2(\alpha) + K_{eq,N} \cdot \sin^2(\alpha) \tag{15}$$

where $K_{eq,Q}$ is the joint-bolt shear stiffness and $K_{eq,N}$ is the joint-bolt tensile stiffness, when the bolt is perpendicular to the plane of the joint; α is an inclination angle of the connecting bolt.

Based on the relative displacement direction and the tensile state of the bolt, there are two basic models for the joint shear deformation: the tensile model and the no tensile one, because there is no constraint on the bolt head when the bolt is compressed along the axial direction.

When the joint deformation follows the no tensile model, the shear stiffness K_{eq} can be obtained by the shear stiffness of the joint:

$$K_{eq} = K_{eq,Q} \cdot \cos^2(\alpha) \tag{16}$$

Based on the results of Han et al. (2023d), the joint-bolt tensile stiffness has a constant value (the green line in Figure 2), and the joint-bolt shear stiffness has a nonlinear trend varying the relative displacement between the segments (the blue lines in the figure).

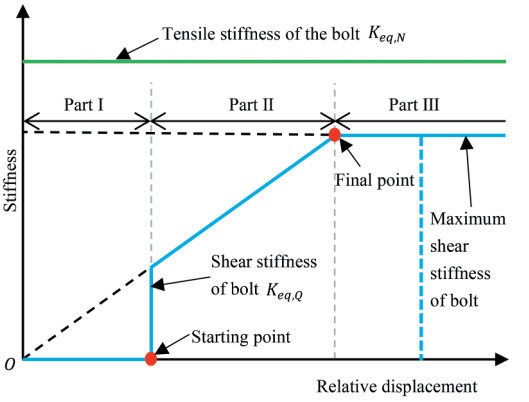

Figure 2. The joint-bolt tensile stiffness and the shear stiffness when the bolt is perpendicular to the plane of the joint (after Han et al., 2023d).

The tensile stiffness of the joint can be obtained by the following equation:

$$K_{eq,N} = \frac{1}{\frac{\coth(\rho \cdot l_{thread})}{E_b \cdot A_b \cdot \rho} + \frac{l_{shank}}{E_b \cdot A_b} + \frac{1}{K_{x,o}}} \tag{17}$$

where l_{thread} is the length of the thread part of the bolt which is installed inside a concrete bolt hole, l_{shank} is the length of the shank part of the bolt. Parameter ρ can be obtained by the following equation:

$$\rho^2 = \frac{\beta_c \cdot \pi \cdot d_b}{E_b \cdot A_b} \tag{18}$$

where β_c is the concrete foundation shear modulus, d_b is the diameter of the bolt. $K_{x,o}$ represents the compressive stiffness of the concrete surface under the application of the washer of the bolt head.

$$K_{x,o} = k_c \cdot \frac{\pi}{4} \cdot \left(d_{washer}^2 - d_h^2\right) \tag{19}$$

where d_{washer} and d_h are the diameter of the washer and the bolt hole, respectively; k_c is the concrete foundation compressive modulus. The parameters k_c and β_c can be determined by laboratory tests and are discussed in the references (Han et al., 2023b).

The shear stiffness of the joint has three parts, and also includes three key parameters: a maximum shear stiffness, locations of a starting point and of a final point. The maximum value of the shear stiffness can be obtained by the following equation:

$$K_{eq,Q,max} = 2 \cdot E_b \cdot I_b \cdot \beta^3 \cdot |\eta| \tag{20}$$

where I_b is the moment of inertia of the bolt cross-section, η and β are two parameter; β depends on the concrete foundation compression modulus:

$$\beta = \sqrt[4]{\frac{k_c \cdot d_b \cdot 1000}{4 \cdot E_b \cdot I_b}} \tag{21}$$

the η parameter depends on the bolt length and on β: the detailed derivation of them can be seen in Han et al., 2023d.

The location of the starting point can be obtained by the following equation:

$$L_{start} = \frac{d_{max,h,l} - d_b}{2} \cdot \frac{l_{shank}^3}{l_{bolt,l}^2 \cdot \left(3 \cdot l_{shank} - 2 \cdot l_{bolt,l}\right)} \cdot \frac{1}{\cos(\alpha)} \tag{22}$$

The location of the final point is equal to the sum of the length of part I and part II.

$$L_{final} = L_{start} + L_{partII} \cdot \frac{1}{\cos(\alpha)} \tag{23}$$

where $L_{part_{II}}$ is the length of part II:

$$L_{PartII} = \frac{2}{K_{eq,Q}} \cdot \frac{15 \cdot E_b \cdot I_b}{4 \cdot l_{bolt,rs}^3 + 10 \cdot E_b \cdot I_b \cdot \delta \cdot l_{bolt,rs} - 10 \cdot E_b \cdot I_b \cdot \beta \cdot l_{bolt,rs}^2} \cdot \frac{d_{max,h,r} - d_b}{2} \tag{24}$$

where $d_{max,h,l}$, $d_{max,h,r}$, $l_{bolt,l}$ and $l_{bolt,rs}$ are geometrical parameters of the bolt, δ and ω are the middle parameters which can be found in the reference (Han et al., 2023d), where the segment connected with the bolt head is the left one.

The representation of the connecting bolts in the cross section of the segmental lining rings is shown in Figure 3. The green rectangle is the first ring and the white one is the second installed segmental ring. The angle ϑ represents the location of each connecting bolt in the cross section.

The bolts have different angles with the circular joint. The equivalent inclination angle γ is used to represent the angle of the bolt axis with the displacement vector of the lining segment.

2.2.2 *Shear stiffness of a circular joint*

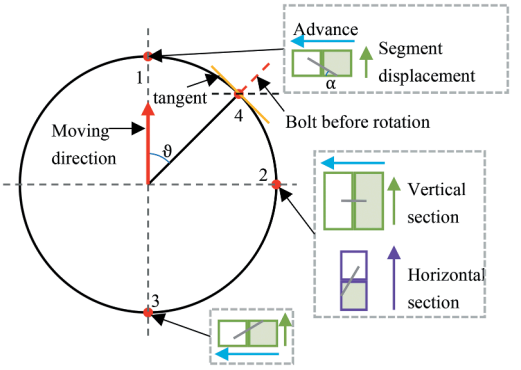

Figure 3. Different axial directions of the bolts in the cross section (after Han et al. (2023d)).

The angle γ of the considered bolt with the location ϑ can be determined by the following equation:

$$\gamma = \arcsin(\sin\alpha \cdot \cos\vartheta) \tag{25}$$

where α is the inclination angle of the bolt at point 1 as shown in Figure 3, ϑ represents the location of the considered bolt in the cross section ($\vartheta \in [0,\ \pi]$).

When $\gamma > 0$, the joint-bolt tensile stiffness can be ignored, and the joint-bolt shear stiffness can be obtained by Equation 16, where the angle α is replaced by γ. When $\gamma \leq 0$, the shear stiffness of the joint can be calculated using Equation 15 by replacing α with γ. Finally, the shear stiffness of the circular joint can be obtained by the summation of the shear stiffness K_{eq} of all the bolts in the lining cross section.

Table 1. The assumed material parameters.

Bolt steel Elastic modulus (GPa)	Bolt Steel Poisson's ratio	Concrete Elastic modulus (GPa)	Concrete Poisson's ratio	Concrete foundation compression modulus (MPa/mm)	Concrete foundation shear modulus (MPa/mm)
206	0.3	35.5	0.2	74.87	10.10

Table 2. The geometrical parameters of the bolting system.

Bolt diameter (m)	Diameter of gasket (m)	Inclination angle of the bolt (°)	Length of the bolt on the left segment (m)	Length of the bolt on the right segment (shank part + thread one) (m, m)	Max and min hole diameter on the left segment (mm, mm)	Max hole diameter (mm)
0.03	0.07	30	0.282	0.06 + 0.19	36, 40	60

The calculated results of the shear stiffness of each bolt are shown in Figure 4 and the one of the whole circular joint with the increase of the relative displacement is shown in Figure 5, where the joint is connected by 19 bolts. The assumed material parameters of the bolt steel and concrete are listed in Table 1 and the structural parameters are listed in Table 2.

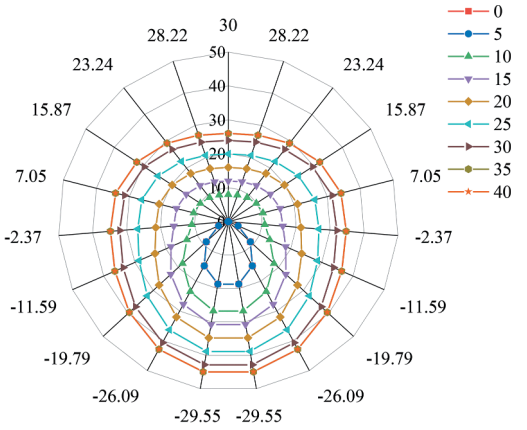

Figure 4. The distribution of the shear stiffnesses on the joint connected by 19 bolts.

From Figure 4, the shear stiffness of all the bolts on the circular joint shows a uniform distribution: the value of the shear stiffness of the joint increases from the top to the bottom. With the increase of the relative displacements of the segments, the shear stiffness of each bolt increases correspondingly. Based on Figure 5, the shear stiffness of the circular joint shows a similar trend with the one of the single bolt, where the minimum shear stiffness of the joint is determined by the joint-bolt tensile stiffnesses of all the bolts.

Based on Equation 13, the shear stiffness of the circular joint can be determined based on the relative displacement of the segments together with the projection length.

The distribution of the shear stiffness on the circular joint is uneven as shown in Figure 4: there are different start points and final points for each bolt varying the equivalent inclination angle γ based on Equation 22, Equation 23 and Equation 25. Considering the uniform distribution of the bolts on the circular joint, a virtual bolt at the location $\vartheta = 45°$ is used to represent the shear stiffness of the circular joint together with the number of bolts. Therefore, the shear stiffness can be derived by Equation 15:

$$\begin{cases} K_N & v_{seg} < L_{s,\vartheta=45°} \\ K_N + K_Q \cdot \frac{v_{seg}}{L_{f,\vartheta=45°}} & L_{s,\vartheta=45°} \le v_{seg} < L_{f,\vartheta=45°} \\ K_N + K_Q & v_{seg} \ge L_{f,\vartheta=45°} \end{cases} \tag{26}$$

where n is the number of bolts on the circular joint, $L_{s,\vartheta=45°}$ and $L_{f,\vartheta=45°}$ are the start point and the finial point when the equivalent inclination angle is equal to $\gamma_{\vartheta=45°}$ at location $\vartheta = 45°$ (Equation 25):

$$\begin{cases} K_N = K_{eq,N} \cdot \sin^2(\gamma_{\vartheta=45°}) \cdot \frac{n}{2} \\ K_Q = K_{eq,Q,max} \cdot \cos^2(\gamma_{\vartheta=45°}) \cdot n \end{cases} \tag{27}$$

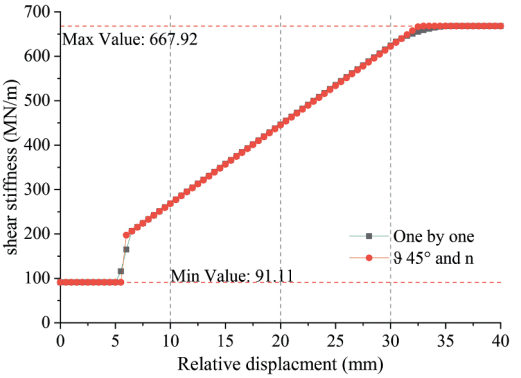

Figure 5. The shear stiffness of a circular joint connected by 19 bolts varying the relative displacements.

Based on Equation 26, the shear stiffness of the circular joint is also shown in Figure 5: a good consistence between the two curves can be seen and Equation 26 can be used to calculate the equivalent shear stiffness of a circular joint.

Based on Equation 13, the equivalent shear stiffness of the joint $(k \cdot G \cdot A)_{eq}$ can be obtained as:

$$(k \cdot G \cdot A)_{eq} = \begin{cases} K_N \cdot L_{bp} & v_{seg} < L_{s,\vartheta=45^\circ} \\ K_N \cdot L_{s,\vartheta=45^\circ} + \left(K_N + K_Q \frac{L_{s,\vartheta=45^\circ} + v_{seg}}{2 \cdot L_{f,\vartheta=45^\circ}}\right) \cdot \left(v_{seg} - L_{s,\vartheta=45^\circ}\right) \cdot L_{bp} & L_{s,\vartheta=45^\circ} \le v_{seg} < L_{f,\vartheta=45^\circ} \\ \frac{K_N \cdot L_{s,\vartheta=45^\circ} + \left(K_N + K_Q \frac{L_{s,\vartheta=45^\circ} + L_{f,\vartheta=45^\circ}}{2 \cdot L_{f,\vartheta=45^\circ}}\right) \cdot \left(L_{f,\vartheta=45^\circ} - L_{s,\vartheta=45^\circ}\right) + \left(K_N + K_Q\right) \cdot \left(v_{seg} - L_{f,\vartheta=45^\circ}\right)}{v_{seg}} \cdot L_{bp} & v_{seg} \ge L_{f,\vartheta=45^\circ} \end{cases} \quad (28)$$

On the basis of Figure 1 and Figure 5, both of the bending stiffness and shear stiffness of a circular joint show a nonlinear behaviour with the relative displacement of the segments on the joint. Considering a nonlinear behaviour of the circular joint, the segmental lining deformation along the longitudinal direction is discussed on the next section.

3 SEGMENTAL LINING DEFORMATION

3.1 *FEM model of segmental lining deformation*

During the construction of a tunnel using the Tunnel Boring Machines (TBMs), the applied forces on the segmental lining can be divided into two classes: the loads along the axial direction of the tunnel, and the ones on the cross section of the tunnel, perpendicular to the axial direction. The forces on the cross section are produced by the slurry (the filling material) and the ground surrounding the tunnel; the mechanical behaviour of the slurry change over time, and the state of the slurry transforms slowly from a liquid state to solid one. When the slurry is in the liquid state, there are great buoyancy forces acting on the segmental lining; the buoyancy effect of the slurry decreases with the hardening phase (Fu et al., 2023). The slurry presence in the model is considered with a fluid zone and a solid one separately (Figure 6). Due to strong constraints by the tail brush inside the TBM tail, a fixed constraint is applied on the first node of the model. For the forces applied along the axial direction of the tunnel, the friction between the lining and the surrounding ground is ignored, and the normal force (axial force in the longitudinal direction) acting on the segmental lining is equal to the applied normal force by the hydraulic jacks: these forces can affect the bending stiffness of the circular joint on the basis of Figure 1.

Based on the Timoshenko theory, a FEM model is adopted to analyse the lining deformation along the longitudinal direction: it represents both the segmental lining rings and circular joints using standard elements and joint elements as shown in Figure 6. With the FEM model, the behaviours of joints and rings can be separately analysed considering the nonlinear behaviour of joints as previously introduced.

On the FEM model (Figure 6), the external forces on each node $[F]$ are equal to the global stiffness matrix $[K]$ multiplied by the corresponding nodal displacements $[S]$:

$$[K] \cdot [S] = [F] \quad (29)$$

The global stiffness matrix can be obtained by composing the local stiffness matrices on each element:

$$[K] = \begin{bmatrix} k_{1,a} & k_{1,b} & 0 & \cdots & 0 & 0 \\ k_{1,c} & k_{1,d} + k_{2,a} & k_{2,b} & \cdots & 0 & 0 \\ 0 & k_{2,c} & k_{2,d} + k_{3,a} & \cdots & 0 & 0 \\ \vdots & \vdots & \vdots & \ddots & 0 & 0 \\ 0 & 0 & 0 & \cdots & k_{n-1,d} + k_{n,a} & k_{n,b} \\ 0 & 0 & 0 & \cdots & k_{n,c} & k_{n,d} \end{bmatrix} \quad (30)$$

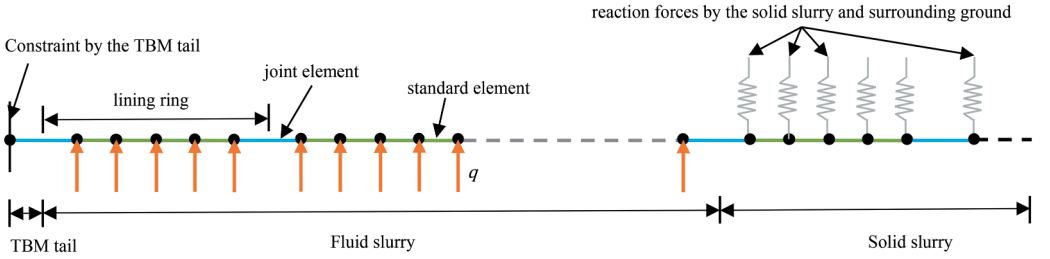

Figure 6. The numerical elements of the segmental lining model with the applied constraints (after Han et al., 2023c).

where the terms of the stiffness matrix depend on the element stiffness matrix:

$$[k_E]_i = \begin{bmatrix} k_{i,a} & k_{i,b} \\ k_{i,c} & k_{i,d} \end{bmatrix} = \frac{EI}{l^3} \begin{bmatrix} \frac{12}{1+\Phi} & \frac{6l}{1+\Phi} & -\frac{12}{1+\Phi} & \frac{6l}{1+\Phi} \\ \frac{6l}{1+\Phi} & \frac{4+\Phi}{1+\Phi} l^2 & -\frac{6l}{1+\Phi} & \frac{2-\Phi}{1+\Phi} l^2 \\ -\frac{12}{1+\Phi} & -\frac{6l}{1+\Phi} & \frac{12}{1+\Phi} & -\frac{6l}{1+\Phi} \\ \frac{6l}{1+\Phi} & \frac{2-\Phi}{1+\Phi} l^2 & -\frac{6l}{1+\Phi} & \frac{4+\Phi}{1+\Phi} l^2 \end{bmatrix} \tag{31}$$

where Φ is the ratio between the bending stiffness (EI) and shear stiffness (kGA) of elements based on Timoshenko theory:

$$\Phi = \frac{12 \cdot (EI)}{(kGA) \cdot l^2} \tag{32}$$

For the standard element, the bending stiffness and shear stiffness depend on the material of the segmental ring (concrete),, $(kGA) = (k \cdot G_{con} \cdot A)$, k is the shear coefficient based on the Timoshenko theory.

For the joint element, the bending stiffness (EI) can be determined based on Figure 1 and the shear stiffness (kGA) depends on Figure 5 with the relative displacement of segments.

Before the hardening of the slurry, the state of slurry is liquid. The length of the liquid zone is determined by the speed of the TBM excavation v and by the hardening time of slurry t_0:

$$d = v \cdot t_0 \tag{33}$$

The buoyancy force can be quickly evaluated with the Archimedes' principle based on the specific weight of the slurry γ_{sl} and of the concrete ring γ_{con}:

$$q = \gamma_{sl} \cdot \frac{\pi}{4} \cdot D_e^2 - \gamma_{con} \cdot \frac{\pi}{4} \cdot \left[D_e^2 - (D_e - 2t)^2 \right] \tag{34}$$

In the FEM model, the influence of the solid slurry and of the surrounding ground can be considered by adding a series of additional springs connected to the nodes in the global stiffness matrix $[K]$ along the main diagonal (Oreste, 2007). The additional terms can be obtained by the following equation:

$$[k_w]_{i,a} = \begin{bmatrix} k_w \cdot l_{av,i} & 0 \\ 0 & 0 \end{bmatrix} \tag{35}$$

where $l_{av,i}$ is the average length of the elements around the node i, and k_w is the spring stiffness considering the stiffness of the solid slurry and of the ground; it can be determined by the following equation (Han et al., 2023c):

$$k_w = \gamma_G \cdot (50 \cdot h_0 - 6.25\pi \cdot D_e) \tag{36}$$

where γ_G is the bulk density of the ground, h_0 is the depth of the tunnel axis from the ground surface.

Based on Equation 8 and Equation 28, the bending stiffness of the joint depends on the bending moment and on the normal force acting on the joint; the shear stiffness of the joint depends on the relative displacement of segments on the joint. An iterative procedure needs to be adopted to analyse the deformations of the segmental lining along the longitudinal direction.

The FEM model can be calculated on the basis of the following procedure:

Step 1: calculating the moment M_0 and the relative displacement v_0 of each joint considering JBSE equal to 1 and the shear stiffness of the joint at its maximum value;

Step 2: based on Equation 8 and Equation 28, calculating the new bending stiffness and the shear stiffness of each joint, and also the new moment M_1 and the relative displacement v_1; furthermore, the new average value of the moment between M_0 and M_1, and the relative displacement $\overline{v_1}$ can be obtained;

Step 3: calculating the new bending stiffness and new shear stiffness by Equation 8 and Equation 28, and also the moment M_i and the relative displacement v_i, where $i = 2,\ 3,\ 4 \ldots$.

Step 4: comparing the new moment M_i and relative displacement v_i with the corresponding average values $\overline{M_{i-1}}$ and $\overline{v_{i-1}}$; when the biggest differences of the moments and the relative displacements are larger than a specific value, the average value $\overline{M_i}$ and $\overline{v_i}$ can be obtained and substituted into the step 3 and so on; otherwise, finishing the iterative procedure.

3.2 *The influence of the circular joint stiffnesses*

Based on the developed FEM model, the segmental lining deformation along the longitudinal direction can be obtained for a real case, with an external diameter of the tunnel of 8.5m, a thickness of the lining of 0.4m and a length of the ring 1.6m. The densities of the slurry and of the segmental lining are 1938kg/m^3 and 2500kg/m^3, respectively; the density of the ground is 1800kg/m^3 and the depth of the tunnel from ground surface is 15m. The assumed advancing speed of the TBM is 0.5m/h, and the hardening time of the slurry is 15h. The material and structural parameters of the connecting bolt and of the bolt hole is the same as Table 1 and Table 2. The JBSE and the shear stiffness of the joints along the longitudinal direction are shown in Figure 7 and Figure 8.

From Figure 7, the normal force has a significant influence on the joint bending stiffness. When the normal force is equal to 0, the joint has a low bending stiffness. With the increase of the normal force, the bending stiffness of the joint also increases. However, the distribution of the bending stiffness is not uniform, and the joints close to the fluid slurry zone have low stiffness values. When the normal force is larger than 5MN, only the first joints have a lower bending stiffness than the rings; most of the bending stiffness values of joints are close to the one of the ring.

Based on Figure 8, the shear stiffnesses decrease from the first joint within the fluid slurry zone, and the

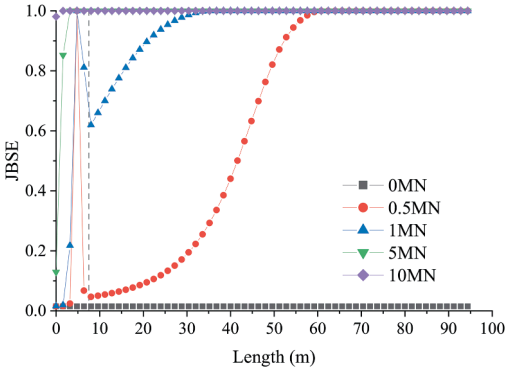

Figure 7. The JBSE value of the joint along the longitudinal direction, for different values of normal forces.

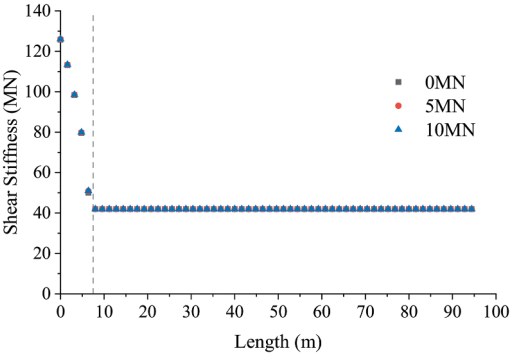

Figure 8. The shear stiffness of the circular joint along the longitudinal direction, for different values of normal forces.

values keep as a constant in the solid slurry zone; the normal force has no effect on the shear stiffness. Therefore, the thrust force has a slight influence on the vertical displacements of the segmental lining, while influencing the bending deformation; the fluid slurry zone has a significant effect on the uplift displacement. The influence of the length of the fluid slurry zone is shown in Figure 9 and Figure 10, where the hardening times of slurry are taken 1h, 5h, 10h and 15h separately.

In Figure 9 the joints show a significant displacement than rings: it means that the uplift displacement of segmental linings is caused by the relative displacements of joints in the fluid slurry zone. In Figure 9 the hardening time of the slurry has a significant influence on the vertical displacements of segmental lining. When the hardening time of the slurry is reduced, the buoyancy phenomenon in the liquid slurry decreases (Figure 10): it causes a reduction of the relative displacement of the first joint as shown in Figure 9.

The density of the slurry is another factor affecting the buoyancy phenomenon. The vertical displacement of the segmental lining along the longitudinal direction is shown in Figure 11 with different slurry densities.

From Figure 11, the vertical displacements of the segmental lining along the longitudinal direction

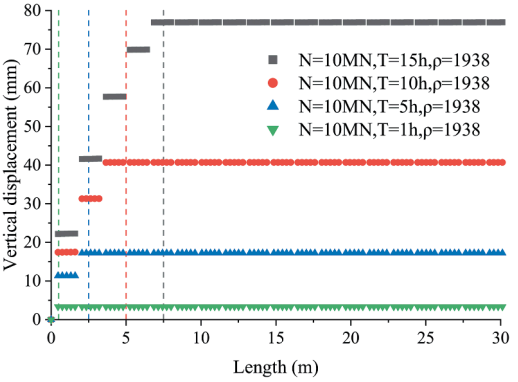

Figure 9. Vertical displacements of the segmental lining for different slurry hardening times varying the distance from the TBM tail.

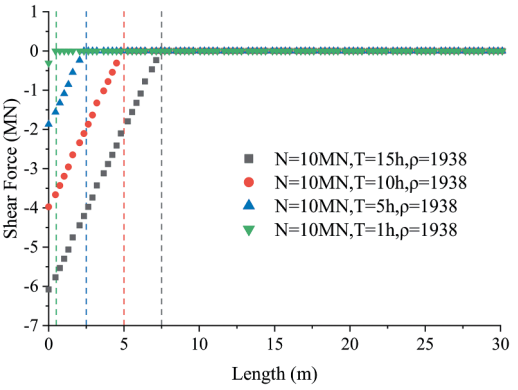

Figure 10. The shear forces on the segmental lining for different slurry hardening times varying the distance from the TBM tail.

decrease with the decrease of the slurry density in the fluid slurry zone. The reduction of the vertical displacement increases when the density of the slurry varies from 1600 to 1200kg/m^3 and from 1200 to 800kg/m^3.

Based on the results of Figure 9 and Figure 11, reducing the hardening time and the density of the slurry is a useful technique to decrease the uplift displacement of the tunnel lining.

4 CONCLUSIONS

Focusing on the nonlinear behaviour of segmental lining joints, calculation methods for the bending stiffness and shear stiffness of circular joints are discussed, and the effect of the slurry presence on the segmental lining deformation along the longitudinal direction is analysed.

1. The bending stiffness of joints is discussed, and the a calculation method is developed. The bending stiffness of joints is determined by the normal forces and the moment applied on the joint: the

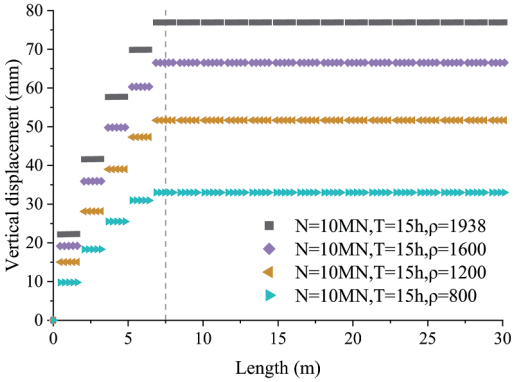

Figure 11. Vertical displacements of the segmental lining with different slurry densities varying the distance from the TBM tail.

value of the bending stiffness decreases with the increase of the moment.

2. A simplified method for the evaluation of the joint shear stiffness with a single bolt is developed. Considering that the shear stiffnesses of inclined bolts are not uniform, the equation of the shear stiffness of a circular joint is proposed. Based on the calculated results of the shear stiffness, the joint shear stiffness increases with the relative displacement of the joint.
3. Considering the nonlinear behaviour of joints, a FEM model based on the Timoshenko beam theory is introduced and an iterative procedure is adopted to calculate the segmental lining deformation along the longitudinal direction. The FEM model can successfully evaluate the deformation of the rings and the joint separately.
4. Based on the calculated results, the normal force shows an obvious influence on the bending stiffness of joints, but no effect on their shear stiffness. The vertical displacements of the lining are mainly influenced by the relative displacements of the joints. Furthermore, decreasing the hardening time and the density of the slurry the vertical displacements of the segmental lining can be reduced.

ACKNOWLEDGMENTS

This study was financially supported by the Fundamental Research Funds for the Central Universities, CHD (Grant No. 300102212702), and this support is gratefully acknowledged. The first author also would like to appreciate the scholarship from China Scholarship Council (Grant No. 202106560030) for his study in Politecnico di Torino.

REFERENCES

Chen, R.P., Meng, F.Y., Ye, Y.H., Liu, Y., 2018. Numerical simulation of the uplift behavior of shield tunnel during construction stage. Soils Found. 58, 370–381.

Cheng, H.Z., Chen, R.P., Wu, H.N., Meng, F.Y., Yi, Y.L., 2021. General solutions for the longitudinal deformation of shield tunnels with multiple discontinuities in strata. Tunn. Undergr. Space Technol. 107.

Fu, Y., Mei, C., Chen, X., Li, W., Yu, B., Li, X., Wang, B., Wang, S., 2023. The time-dependent grout buoyancy behavior based on cement hydration mechanism. Cem. Concr. Res. 166.

Gong, C., Yang, J., Fu, J., 2020. Characteristics and Influencing Factors of Segment Cracking of Large-Diameter River-Crossing Shield Tunnelling in Composite Rock Strata. Modern Tunnelling Technology 57, 30–42.

Guo, W., Feng, K., Zhou, Y., Lu, X., Qi, M., He, C., Xiao, M., 2023a. Experimental and numerical investigation on the shear behavior and damage mechanism of segmental joint under compression-shear load. Tunn. Undergr. Space Technol. 139.

Guo, W., Feng, K., Zhou, Y., Yang, W., Lu, X., Xiao, M., He, C., 2023b. Full-scale test and numerical modeling on deformation and damage behavior of segmental joints under ultimate compression-bending load. Eng. Struct. 279.

Han, X., Oreste, P., Ye, F., 2023a. The buoyancy of the tunnel segmental lining in the surrounding filling material and its effects on the concrete stress state. Geotech. Geol. Eng. 41, 741–758.

Han, X., Oreste, P., Ye, F., 2023b. The contribution of the bolting system to the shear stiffness of circumferential joints in tunnel segmental linings. Comput. Geotech. 162, 1–21.

Han, X., Oreste, P., Ye, F., 2023c. The important role of stiffnesses values of circular joints on the stress state developed in the tunnel segmental lining. Geomech. Geophys. Geo-Energy Geo-Resour. 9, 1–32.

Han, X., Oreste, P., Ye, F., 2023d. The influence of the nonlinear behaviour of connecting bolts on the shear stiffness of circular joints in a tunnel segmental lining, Submitted to Journal.

Li, X., Zhou, X., Hong, B., Zhu, H., 2019. Experimental and analytical study on longitudinal bending behavior of shield tunnel subjected to longitudinal axial forces. Tunn. Undergr. Space Technol. 86, 128–137.

Liu, X., Dong, Z.B., Song, W., Bai, Y., 2018. Investigation of the structural effect induced by stagger joints in segmental tunnel linings: Direct insight from mechanical behaviors of longitudinal and circumferential joints. Tunn. Undergr. Space Technol. 71, 271–291.

Lu, D., 2020. Analysis on mechanical characteristics and cracking pehnomena of segment structure for shield tunnel during construction period. Southwest Jiaotong University.

Oreste, P., 2007. A numerical approach to the hyperstatic reaction method for the dimensioning of tunnel supports. Tunn. Undergr. Space Technol. 22, 185–205.

Shiba, Y., Kawashima, K., Obinata, N., Kano, T., 1988. An evaluation method of longitudinal stiffness of shield tunnel linings for application to seismic response analyses. J. Jpn. Soc. Civ. Eng, 319–327.

Zhou, S.H., Ji, C., 2014. Tunnel segment uplift model of earth pressure balance shield in soft soils during subway tunnel construction. Int. J. Rail Transp. 2, 221–238.